Copper binding by a unique family of metalloproteins is dependent on kynurenine formation

Anastasia C. Manesis[a,b], Richard J. Jodts[a,b], Brian M. Hoffman[a,b], and Amy C. Rosenzweig[a,b,1]

[a]Department of Molecular Biosciences, Northwestern University, Evanston, IL 60208; and [b]Department of Chemistry, Northwestern University, Evanston, IL 60208

Contributed by Amy C. Rosenzweig, April 21, 2021 (sent for review January 13, 2021; reviewed by Kenneth D. Karlin and Aimin Liu)

Some methane-oxidizing bacteria use the ribosomally synthesized, posttranslationally modified natural product methanobactin (Mbn) to acquire copper for their primary metabolic enzyme, particulate methane monooxygenase. The operons encoding the machinery to biosynthesize and transport Mbns typically include genes for two proteins, MbnH and MbnP, which are also found as a pair in other genomic contexts related to copper homeostasis. While the MbnH protein, a member of the bacterial diheme cytochrome *c* peroxidase (bCcP)/MauG superfamily, has been characterized, the structure and function of MbnP, the relationship between the two proteins, and their role in copper homeostasis remain unclear. Biochemical characterization of MbnP from the methanotroph *Methylosinus trichosporium* OB3b now reveals that MbnP binds a single copper ion, present in the +1 oxidation state, with high affinity. Copper binding to MbnP in vivo is dependent on oxidation of the first tryptophan in a conserved WxW motif to a kynurenine, a transformation that occurs through an interaction of MbnH with MbnP. The 2.04-Å-resolution crystal structure of MbnP reveals a unique fold and an unusual copper-binding site involving a histidine, a methionine, a solvent ligand, and the kynurenine. Although the kynurenine residue may not serve as a Cu^{I} primary-sphere ligand, being positioned ∼2.9 Å away from the Cu^{I} ion, its presence is required for copper binding. Genomic neighborhood analysis indicates that MbnP proteins, and by extension kynurenine-containing copper sites, are widespread and may play diverse roles in microbial copper homeostasis.

copper | diheme peroxidase | kynurenine | methanotroph | MbnP

Copper is vital to the physiology of aerobic methanotrophic bacteria, organisms that utilize methane gas as their sole carbon source (1). In the first step of their metabolic pathway, methane is converted to methanol by methane monooxygenase (MMO) enzymes, of which there are two types (2, 3). The copper-containing particulate MMO (pMMO) is utilized by almost all known methanotroph species, whereas the iron-containing soluble MMO is expressed in a subset of methanotrophs under conditions of copper starvation (4). As the primary enzyme responsible for biological methane oxidation, pMMO is produced in high quantities, comprising up to 20% of cellular protein mass (5). Given that pMMO activity is dependent on copper (6), methanotrophs have an unusually high copper requirement and have proven to be fertile ground for the discovery of new copper acquisition systems and copper-binding proteins.

One way that some methanotrophs obtain copper is by production and secretion of methanobactins (Mbns), ribosomally synthesized, posttranslationally modified peptide natural products that bind Cu^{I} with high affinity (7). The protein machinery to manufacture and transport Mbns is encoded by operons, which are down-regulated under copper-replete conditions (8). The copper-bound form of Mbn, CuMbn, is reinternalized by an active transport process involving the TonB-dependent transporter MbnT (9, 10). How CuMbn releases its tightly bound Cu^{I} cargo for use by pMMO is not known and could involve redox chemistry, conformational changes, and one or more periplasmic copper-binding proteins (10–12). While many of the proteins encoded by Mbn operons have been assigned functions (9, 10, 13, 14), the roles of two proteins, MbnP and MbnH, remain unclear. These proteins, encoded as a gene pair in four out of five Mbn operon families, are referred to as the "metallo-mystery pair" in the TIGRFAM database (15) and have been proposed to play a role in copper release from Mbn (12).

MbnH is a member of the bacterial diheme cytochrome *c* peroxidase (bC*c*P)/MauG family (PF03150) and belongs to a distinct and divergent group within a broader subfamily that encompasses MauG-like diheme enzymes (16). In MauG, dual heme groups, one high-spin and one low-spin, generate a highly reactive *bis*-Fe^{IV} catalytic intermediate that oxidizes two tryptophan residues in the methylamine dehydrogenase (MADH) precursor protein (preMADH) to form a tryptophan tryptophylquinone cofactor (17). Like MauG, MbnH exhibits a near-infrared (nIR) spectral feature characteristic of charge resonance (CR) bands involving aromatic cation radicals. In MauG, rapid electron transfer between the two heme groups through an intervening tryptophan residue stabilizes the *bis*-Fe^{IV} species, a phenomenon called CR stabilization (17–19). In addition to CR stabilization, MbnH may also be similarly capable of forming a *bis*-Fe^{IV} intermediate upon oxidation with peroxide (16), but the reactivity and potential substrate of this intermediate have not been established.

In contrast to MbnH, MbnP does not belong to a known protein family and contains no recognizable domains (16). Sequence analysis predicts that MbnP proteins are periplasmic, with six highly conserved cysteines, two highly conserved histidines, and a highly conserved WxW motif (Fig. 1 *A* and *D*) (16). There is a strong genetic association of MbnP and MbnH, with ∼88.1% of

Significance

Copper is particularly important in the metabolism of methanotrophs, methane-consuming bacteria that have potential applications in converting methane, a greenhouse gas, to useful fuels and chemicals. How methanotrophs and other bacteria acquire and distribute copper, which is toxic in excess, is not well understood. Here we identify and characterize a previously unknown copper-binding protein implicated in methanotroph copper homeostasis. This protein, MbnP, binds copper with an unusual coordination sphere that includes kynurenine, a tryptophan oxidation product that is produced in vivo by a partner protein, MbnH. MbnP is the founding member of a widespread protein family with potentially broad roles in microbial copper homeostasis.

Author contributions: A.C.M., R.J.J., and A.C.R. designed research; A.C.M. and R.J.J. performed research; A.C.M. contributed new reagents/analytic tools; A.C.M., R.J.J., B.M.H., and A.C.R. analyzed data; and A.C.M., R.J.J., and A.C.R. wrote the paper.

Reviewers: K.D.K., Johns Hopkins University; and A.L., The University of Texas at San Antonio.

The authors declare no competing interest.

[1]To whom correspondence may be addressed. Email: amyr@northwestern.edu.

This article contains supporting information online at https://www.pnas.org/lookup/suppl/doi:10.1073/pnas.2100680118/-/DCSupplemental.

Published May 31, 2021.

mbnP genes within two genes of *mbnH* (Fig. 1*B*). These *mbnPH* pairs are not only present in Mbn operons but also found in proximity to genes that encode a range of copper-binding proteins and membrane transporters, including CopC, CopD, and PCu_AC. Three *mbnPH* pairs are found in the methanotroph *Methylosinus* (*Ms.*) *trichosporium* OB3b, one in the Mbn operon, and two in additional operons encoding MbnT, MbnP, and MbnH; all are regulated by copper (7, 10, 16, 20).

The presence of conserved tryptophan residues in MbnP and its genetic association with a MauG-like protein, MbnH, are reminiscent of the methanotroph copper-binding proteins *Methylococcus* (*M.*) *capsulatus* (Bath) MopE* (a truncated and secreted form of the MopE protein) and CorA, a copper-repressible protein from *Methylomicrobium album* BG8 (21–23). Crystal structures of MopE* and CorA are nearly identical and revealed a Cu^I binding site involving two histidine residues and a kynurenine, which is an oxidation product of tryptophan (Fig. 2) (21, 22). Expression of both proteins, along with that of a homolog from *Methylomicrobium alcaliphilum* 20Z (21, 24), is negatively regulated by copper, and genetic disruption studies are consistent with a role in copper acquisition (25). While the mechanism by which these proteins acquire a kynurenine residue has not been addressed, all are present in the genomes as pairs with predicted diheme cytochrome *c* peroxidases, often referred to as CorB proteins. Despite this parallel, there is no obvious relationship between MopE*/CorA proteins and MbnP.

By analogy to MauG and the MopE*/CorA/CorB proteins, we previously suggested that MbnH might oxidize a tryptophan residue in MbnP, perhaps facilitating a copper-handling function related to Mbn (12, 16). Here we show that coexpression of *Ms. trichosporium* OB3b MbnH and MbnP results in a Cu^I-loaded form of MbnP, $MbnP^H$, establishing MbnP as a copper-binding protein. The 2.04-Å-resolution crystal structure of $MbnP^H$ reveals a protein fold that is completely different from MopE*/CorA and an unusual Cu^I binding site containing a kynurenine derived from a tryptophan residue. Taken together, these results suggest that $MbnP^H$ represents a new class of copper-binding proteins with potentially broad roles in microbial copper homeostasis.

Results and Discussion

$MbnP^H$ Is a Copper-Binding Protein. MbnP consists of an N-terminal signal sequence followed by a periplasmic protein sequence (16). Heterologous expression of this full protein sequence from *Ms. trichosporium* OB3b, substituting the native signal sequence with a PelB leader sequence, resulted in ~3 mg/L of pure protein in the soluble fraction (*SI Appendix*, Fig. S1). Size-exclusion chromatography with multiangle light scattering (SEC-MALS) data indicate that the purified MbnP is primarily monomeric in solution (Fig. 3) with no appreciable copper bound; only ~2.5% of the total monomer contains copper according to inductively coupled plasma mass spectrometry (ICP-MS) measurements (Fig. 4*A*). However, the majority of expressed MbnP was found in inclusion

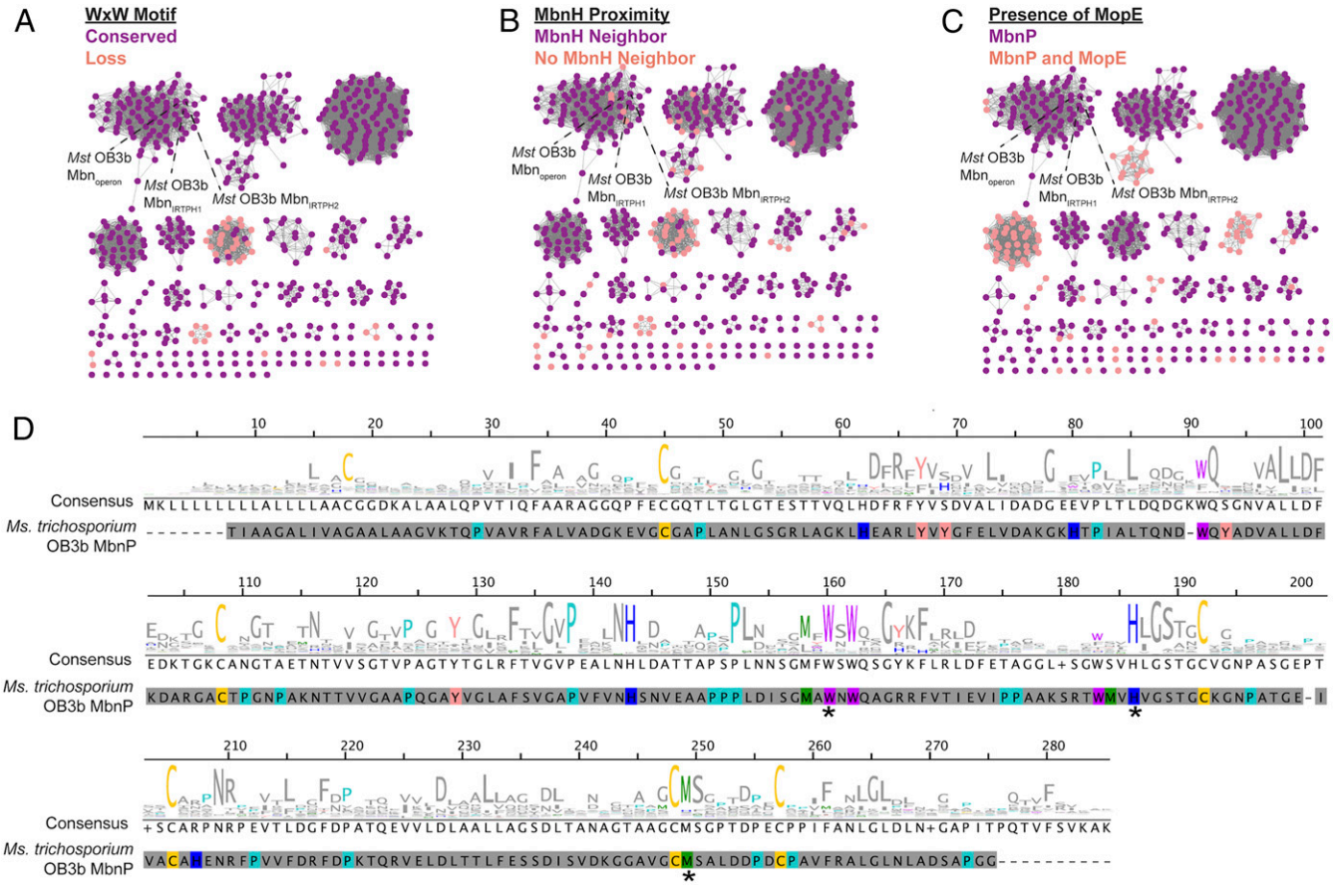

Fig. 1. Sequence similarity network of MbnP. Sequences with 100% identity were clustered into representative nodes, and an E-value cutoff of 1E-70 was used to create the network. (*A*) Conservation of the WxW motif visualized on the SSN network. (*B*) Genetic proximity of MbnP to MbnH visualized on the same SSN. Loss of the WxW motif is almost exclusively observed in MbnPs that are not associated with an MbnH. (*C*) Occurrence of MopE in organisms that also contain MbnP. Organisms containing both MopE and MbnP contain only MbnPs outside of Mbn operons. (*D*) Sequence conservation logo for MbnP. Sequences from representative nodes were aligned against an MbnP profile HMM constructed from representative nodes clustered at 50% sequence identity to produce the logo. Copper-coordinating ligands are denoted with an asterisk.

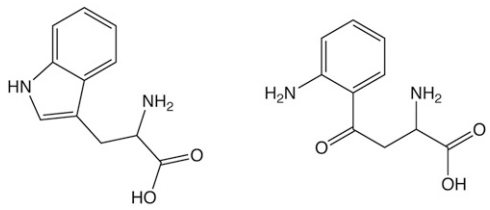

Fig. 2. Chemical structures of tryptophan and kynurenine. Chemical structure of tryptophan (*Left*) compared with kynurenine (*Right*). The bond between the Nε1 and Cδ1 atoms is broken in kynurenine.

bodies, and attempts at refolding were unsuccessful. Given the high rate of cooccurrence of the *mbnP* and *mbnH* genes (Fig. 1*B*), we attempted to increase the yield and stability of MbnP by coexpression with MbnH. The yield of coexpressed MbnP, denoted MbnP^{H}, was ∼10 mg/L, with significantly more protein found in the soluble fraction. The optical spectrum of purified, His$_6$-tagged MbnP^{H} differs from that of His$_6$-tagged MbnP, with new features appearing in the ultraviolet (UV) region at 260 nm and 330 nm (Figs. 3 and 4*B*). These UV features are also observed for strep-tagged MbnP^{H}, indicating that they do not arise from an interaction with the affinity tag (*SI Appendix*, Fig. S2). In contrast to MbnP, coexpressed MbnP^{H} is a dimer in solution (Fig. 3) regardless of the affinity tag used (*SI Appendix*, Fig. S2). Most importantly, ICP-MS indicates that ∼90% of the MbnP^{H} protein is loaded with one copper ion per protein monomer (Fig. 4*A*).

To determine whether the bound copper is in the +1 or +2 oxidation state, a sample of as-isolated MbnP^{H} was examined by CW X-band electron paramagnetic resonance (EPR) at 20 K. The absence of a Cu^{II} signal implies that the bound copper is in the +1 oxidation state (*SI Appendix*, Fig. S3*A*). Attempts to oxidize the Cu^{I} to Cu^{II} using mild oxidants such as hydrogen peroxide were unsuccessful (*SI Appendix*, Fig. S3*B*), indicating that the Cu^{I} state is strongly stabilized. Oxidation to Cu^{II} instead required addition of the strong one-electron oxidant K_2IrCl_6. After the addition of 4 mM K_2IrCl_6, an S = 1/2 Cu^{II} signal appears with well-resolved $^{63/65}$Cu hyperfine splitting at $g_{||}$ of $A_{||}$ = 190 G (585 MHz) and splittings at $g_{\perp}$ of ∼15 G (∼40 MHz), undoubtedly from coordinated nitrogen (*SI Appendix*, Fig. S3*B*). Samples were also examined at Q-band, which eliminates overlap from the K_2IrCl_6 signal but obscures the ^{14}N splittings (*SI Appendix*, Fig. S4). Simulations of the oxidized MbnP^{H} spectrum yielded g-values of 2.25, 2.06, and 2.05 with a $^{63/65}$Cu hyperfine splitting of $A_{||}$ = 590 MHz. Spin quantification of samples against a copper standard at Q-band yields a Cu^{II} concentration of 585 μM, indicating ∼73% conversion from the reduced to the oxidized state.

To investigate the affinity of MbnP^{H} for Cu^{I}, bathocuproine disulfonic acid (BCS) was titrated into MbnP^{H}. BCS is known to form a stable 2:1 complex with Cu^{I} with an association constant of $\beta = K_1K_2$ of $10^{19.8}$ M^{-2} (26). Following the addition of each titrant, the solution was equilibrated at room temperature for 20 min prior to measuring the absorbance (27). The addition of increasing amounts of BCS is accompanied by the appearance of a 483-nm absorbance feature, attributable to the Cu^{I}[BCS]$_2^{3-}$ complex (*SI Appendix*, Fig. S5) (26). Analysis of these data yields an approximate log(K_d) of −17.9 ± 0.097 (K_d [dissociation constant] value of ∼10^{-18} M) for Cu^{I} binding to MbnP^{H} (*SI Appendix*, Table S1). This K_d value for Cu^{I} is comparable to that for a range of Cu^{I} transport proteins (26, 28) and two orders of magnitude greater than what has been observed for MopE* (21, 22), suggesting that MbnP^{H} binds Cu^{I} with lower affinity than MopE*.

The observation that MbnP^{H} only binds copper when coexpressed with MbnH is consistent with the hypothesis that MbnH interacts with and posttranslationally modifies MbnP to generate a copper-binding site. We were not able to isolate a stable complex of MbnP and MbnH by affinity chromatography, suggesting that the interaction between the two proteins is weak, or transiently formed in the cell. To further assess the link between MbnP^{H} copper binding and the action of MbnH, MbnP was coexpressed with an MbnH variant in which heme pocket residue Glu136 is replaced with glutamine. This variant is unable to stabilize an oxidizing intermediate, as evidenced by the lack of the CR stabilization feature in the nIR region upon reaction with H_2O_2 (*SI Appendix*, Fig. S6). The resultant MbnP$^{E136Q\ H}$ did not contain copper (Fig. 4*A*) and could not be loaded with copper via direct anaerobic addition of Cu^{I} or direct aerobic Cu^{II} after purification. This result is consistent with MbnH being the diheme protein responsible for modifying MbnP to make it capable of copper binding.

Given the parallels to the MopE*/CorA proteins, we hypothesized that the modification MbnH enacts on MbnP could be a tryptophan-to-kynurenine oxidation. Tryptophan and kynurenine exhibit distinct absorption and fluorescence spectra (29–31), which were used to assess the possible presence of kynurenine in MbnP^{H} (*SI Appendix*, Fig. S7). To avoid spectroscopic contributions from the protein environment and from bound Cu^{I}, MbnP proteins were unfolded using sodium dodecyl sulfate (SDS) and dithiothreitol (DTT) and copper was removed using excess BCS. Denatured MbnP^{H} shows three distinct absorbances at 280 nm, 330 nm, and 380 nm (*SI Appendix*, Fig. S7*A*). Excitation at 365 nm gives an emission spectrum with a λ_{max} of 450 nm (*SI Appendix*, Fig. S7*B*), consistent with what has been reported previously for kynurenine fluorescence (31). Denatured W176Y MbnP^{H} exhibits a similar absorption profile (*SI Appendix*, Fig. S7*A*) and although the emission intensity is quenched relative to wild-type MbnP^{H}, the emission maximum at 450 nm is consistent with the presence of a kynurenine residue (*SI Appendix*, Fig. S7*B*). Conversely, the absorption and fluorescence spectra of denatured MbnP, MbnP$^{E136Q\ H}$, and W174Y MbnP^{H} do not have absorption maxima in the near UV, nor do they fluoresce when excited at 365 nm (*SI Appendix*, Fig. S7), indicating that these proteins do not contain a kynurenine

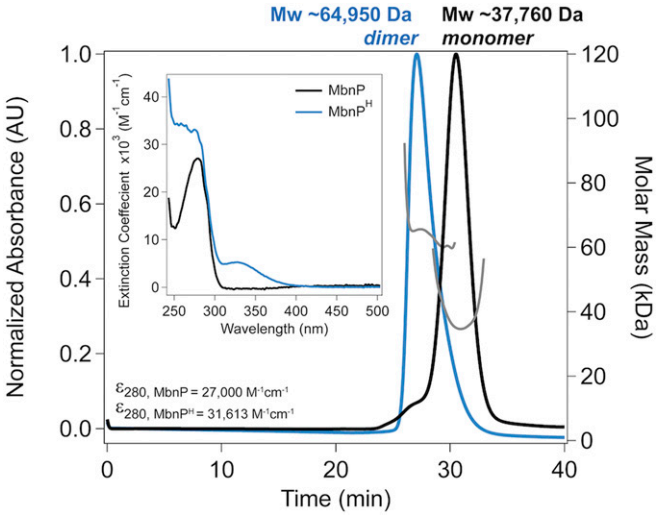

Fig. 3. Oligomerization states of MbnP and MbnP^{H}. SEC-MALS profiles for purified His$_6$-tagged MbnP and MbnP^{H} are shown. (*Inset*) Optical spectra collected at the apex of the predominant peaks. Blue traces indicate the dimeric MbnP^{H} species (molar mass 64,950 Da) and black traces indicate the monomeric MbnP species (molar mass 37,760 Da).

BIOCHEMISTRY

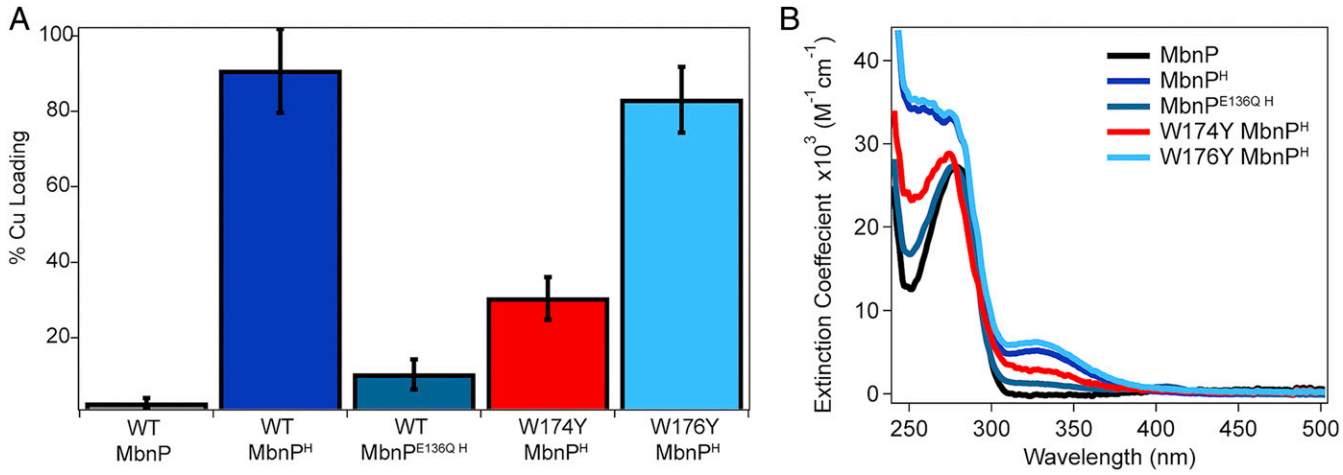

Fig. 4. Metal-binding properties of MbnP. (*A*) Copper content of MbnP and its variants. All samples include a C-terminal His_6 tag. (*B*) Optical spectra of purified MbnP and its variants.

residue. Taken together, these data suggest that kynurenine is required for copper binding by MbnP.

Structural Analysis of MbnP^{H} Reveals a Unique Protein Fold and an Unusual Copper-Binding Site. Both the monomeric His_6-tagged MbnP and dimeric His_6-tagged MbnP^{H} were used for crystallization trials, but crystals were only obtained from the dimeric His_6-tagged MbnP^{H} sample. The crystals belong to space group $P6_1$ with six dimers in the asymmetric unit, and the structure was solved to 2.04-Å resolution by Cu single-wavelength anomalous dispersion (SAD) phasing (*SI Appendix*, Table S2). MbnP^{H} exhibits a previously unobserved protein fold, consisting mainly of β strands (Fig. 5*A*). A central β sheet comprising 11 strands is flanked on one side by the copper center and two β hairpins and on the other side by two α helices and a six-stranded β sheet. Three disulfide bonds are present, involving residues Cys48 and Cys113, Cys213 and Cys225, and Cys268 and Cys277. These are the only cysteines in the sequence and are all highly conserved (Fig. 1*D*) (16). The presence of disulfides is consistent with MbnP's periplasmic localization. The dimer interface includes 760-Å^2 buried accessible surface area and is primarily composed of salt bridges and hydrogen bond interactions (*SI Appendix*, Fig. S8). Although the buried surface area for each dimer pair is significantly higher than that between nondimer pairs, analysis using the PDBePISA webserver results in an interface score of 0 to 0.033, indicating that this dimer is very unlikely to form in vivo (32). If the crystallographic dimer corresponds to the dimer observed by SEC-MALS (Fig. 3), it may be the result of a very weak interaction. In support of this notion, the MbnP^{H} dimer observed by SEC-MALS appears to dissociate partially, as evidenced by significant tailing of the peak. Alternatively, the dimer present in solution may be different from that observed in the crystal structure.

Each protein monomer contains one copper (Fig. 5*B*) and one calcium ion (Fig. 5*C*). In addition, chains E and F also feature ethylene glycol, likely from the cryprotectant solution, near the copper active site. The Ca^{2+} ion is coordinated in a distorted octahedral geometry by the side-chain oxygen atoms of Asp261, Asp274, and Asp276 and the main-chain carbonyl oxygen atoms of Gly263, Ala265, and Gly267 (Fig. 5*C*). This ligand set is typical of a calcium-binding site (33). The copper site is exposed at the surface, with a single copper ion coordinated in a tetrahedral geometry by His207, Met269, a solvent molecule, and a kynurenine ligand (Kyn174) (Fig. 2), apparently produced by posttranslational modification of Trp174 (Fig. 5*B*). Attempts to model the electron density with tryptophan resulted in significant negative difference density on the indole ring, confirming that the bond between the Nε1 and Cδ1 atoms is broken (*SI Appendix*, Fig. S9). Averaged over the six molecules in the asymmetric unit, the Cu-His_{207} Nδ1 distance is 2.11 ± 0.07 Å and the Cu-Met_{269} Sδ distance is 2.40 ± 0.05 Å (*SI Appendix*, Table S3), consistent with covalent interactions.

The Cu-Kyn_{174} N1 distance is 2.93 ± 0.13 Å, calling into question whether this residue should be considered a ligand and whether it is actually necessary for copper binding. Residue 174 is part of the conserved WxW motif that is present in all MbnP sequences except those not found in genomic proximity to MbnH sequences (Fig. 1 *A* and *B*) (16). To determine whether Kyn174 is essential for copper binding, we individually replaced each of the tryptophans in the WxW motif with tyrosine. Replacement of Trp174 by tyrosine significantly reduced the ability of MbnP^{H} to bind copper (30% loading), whereas replacement of Trp176 by tyrosine had very little effect on copper binding (83% loading) (Fig. 4*A*). Therefore, although Kyn174 may be too far from the

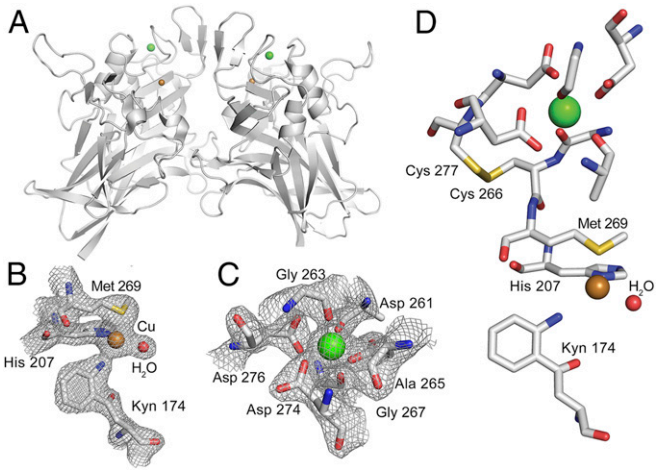

Fig. 5. MbnP^{H} metal centers. (*A*) Overall structure of MbnP^{H} crystallographic dimer showing all the secondary structure elements. Residues in the (*B*) copper-binding site and (*C*) calcium-binding site are shown with the associated electron density maps (*2Fo-Fc*, gray, contoured at 1.6 σ). (*D*) The disulfide bond between Cys266 and Cys277 links the residues in the two metal binding sites.

metal center to form a covalent bond, its presence is required for formation of the copper site. Assuming that Kyn174 is not directly coordinated due to its distance, the ^{14}N hyperfine splittings observed at $g_{\perp}$ in the X-band EPR spectrum of MbnP^{H} after Cu^{I} oxidation to Cu^{II} by K_2IrCl_6 (*SI Appendix*, Fig. S3*B*) likely arise from the coordinated nitrogen of His207. A correlation between g-values and coordination sphere of Cu^{II} confirms that the g-values (*SI Appendix*, Fig. S4) are consistent with methionine ligation as well (34).

Comparison of MbnP^{H} to MopE*/CorA. Although kynurenine is also present in the CorA and MopE* copper sites (21–23), MbnP^{H} bears little resemblance to these two proteins. While MopE* and CorA share an overall fold and metal binding-site locations, MbnP^{H} exhibits a completely different fold (Fig. 6). In addition, the copper and calcium binding sites are 10.2 ± 0.14 Å apart in MbnP^{H} compared to 27.2 Å in MopE* and 27.7 ± 0.05 Å in CorA. Despite the differences in structure, pairwise sequence alignments using MafftWS with preset L-INS-i (accuracy-oriented) mode (35) reveal 18% identity between MopE* and MbnP^{H}, 31% identity between CorA and MbnP^{H}, and 21% identity between CorA and MopE* (*SI Appendix*, Fig. S10). The relationship between homology, structure, and function is not always predictable (36), and it is important to note that MbnP^{H} is periplasmic while MopE* is secreted and CorA is surface-associated. Thus, although MbnP^{H} may be a MopE*/CorA homolog, it likely has a different function, potentially in copper transport rather than copper acquisition from the environment.

Notwithstanding the different locations in the structures, the calcium site in MbnP^{H} is almost identical to those found in MopE* and CorA (21, 22). In all three structures the calcium site is surface inaccessible. This site has been proposed to stabilize the MopE* and CorA structures (21, 22) and likely serves a similar role in MbnP^{H}. Specific to MbnP^{H}, calcium binding may help position Asp276 such that Cys277 can form a disulfide bond with Cys266 (Fig. 5*D*). This disulfide bond then orients Met269 in the copper-binding site. Therefore, calcium binding may directly facilitate copper binding.

The copper-binding site in MbnP^{H} differs from those in MopE* and CorA with respect to ligand identity and coordination geometry. Instead of two histidines and one solvent ligand, the MbnP^{H} site includes one histidine, one methionine, and one solvent ligand (Fig. 6). The copper ion is oriented 0.16 Å and 0.17 ± 0.05 Å (average of six molecules in the asymmetric unit) above the His-Kyn-His plane (toward the solvent) for MopE* and CorA, respectively, yielding almost trigonal planar geometry, consistent with what has been reported for low-coordinate Cu^{I} synthetic compounds (37–40). In MbnP^{H}, the copper ion deviates significantly more out of the plane, measuring 0.68 ± 0.05 Å (average of six molecules in the asymmetric unit) above the His-Met-Kyn plane toward the solvent and is thus more pyramidal in geometry. Of the two amino acid ligands in MbnP^{H}, the histidine is conserved in ∼98% of MbnP sequences whereas the methionine is only conserved in ∼80% (*SI Appendix*, Figs. S11 and S12). Notably, a number of periplasmic copper-trafficking proteins contain methionine ligands. The thioether side chain, excellent as a Cu^{I} ligand, may also facilitate copper exchange in an oxidizing environment (41–43).

Finally, the kynurenines in MopE* and CorA (21, 22) also exhibit longer (∼2.9 Å) Cu–N distances than what would be considered typical for both biological and nonbiological systems (44–46). This distance suggests a relatively weak interaction between the amino group of the kynurenine ligand and the copper ion in all three proteins, and it might be more appropriate to consider the kynurenine a second-sphere, rather than a primary-sphere, ligand. Regardless, it is clear that the oxidation of tryptophan to kynurenine is required for copper binding. It may be that a necessary conformational change occurs upon tryptophan oxidation. Alternatively, having a ligand such as kynurenine might modulate the redox potential of the copper ion and facilitate copper transfer to a physiological partner, specifically if copper is transferred in the +1 oxidation state.

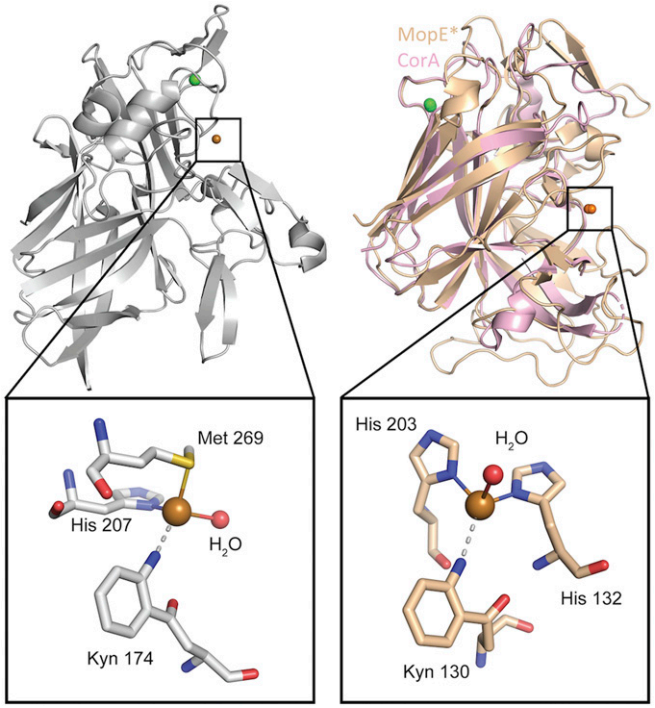

Fig. 6. Comparison of MbnP^{H} to MopE*/CorA. MbnP^{H} (Protein Data Bank [PDB] ID code 7L6G, gray) (*Left*) compared to an overlay of MopE* (PDB ID code 2VOV, tan) with CorA (PDB ID code 4BZ4, pink) (*Right*). (*Insets*) The active sites of MbnP^{H} (gray, *Left*) and MopE* (tan, *Right*).

Potential Functional Roles for MbnP. The discovery that MbnP^{H} is a copper-binding protein is consistent with a role in copper homeostasis. In Mbn-producing methanotrophs, the genomic association of *mbnPH* pairs with *mbnT*s, both within and outside of Mbn operons, and their coregulation by copper (7, 10, 16, 20) imply a role directly related to Mbn trafficking. One possibility is that MbnP extracts copper from Mbn after uptake by MbnT. While the affinity of Mbn for Cu^{I} is in the range of 10^{20} to 10^{21} M^{-1} (11, 47–49), it is possible that conformational changes in Mbn upon interaction with MbnT, MbnP, or both, facilitate release. While MbnP bears some similarity to the extracellular proteins MopE* and CorA, its periplasmic localization precludes it from obtaining copper directly from the environment. MopE* and CorA are found in methanotrophs that lack Mbn operons, including *M. capsulatus* (Bath), *Methylomicrobium album* BG8, and *M. alcaliphilum* 20Z (50), suggesting that they constitute an alternative pathway for copper acquisition. Notably, these Mbn operon-lacking methanotrophs still include *mbnPH* pairs, which are found adjacent to genes coding for PCu_AC (Fig. 1*C*, genomic neighborhoods 1, 2, and 7 in *SI Appendix*, Figs. S13 and S14). Thus, MbnP may play multiple roles in methanotrophs.

As noted previously, *mbnPH* pairs occur in a range of genomic contexts (16). Updated analysis of the *mbnP* genomic neighborhoods reveals 10 distinct neighborhoods of which only two are *mbn* operons (*SI Appendix*, Fig. S14). Therefore, while the majority of Mbn operons contain *mbnPH* (12), most *mbnP* genes are not found within Mbn operons. The genomic presence of MbnP extends well beyond methanotrophs (*SI Appendix*, Fig. S15), suggesting broader

roles across diverse phyla. However, regardless of genomic context, two frequent associations occur. First, *mbnP* is regularly associated with outer membrane importers: 22.3% are adjacent to genes encoding TonB-dependent receptors and another 15.1% neighbor genes encoding β-barrel outer membrane importers that transport hydrophobic compounds. Second, there are multiple gene neighbors that have functions connected to copper homeostasis and/or cuproenzyme assembly (*SI Appendix*, Fig. S14) (16). In addition to the 9.0% of *mbnP* genes that are in Mbn operons, 4.5% are near *copC(D)* genes, and 15.5% are near genes encoding PCu_AC proteins, which are postulated to act as periplasmic copper chaperones (16, 51). It may be that MbnP proteins act more generally to sequester copper and regulate its availability to a range of periplasmic transport pathways. Further investigation of this unusual and widespread protein family is warranted to elucidate its function and to understand the significance of the unusual kynurenine-containing copper site.

Materials and Methods

Bioinformatics. An updated bioinformatic analysis of MbnP was conducted using 1,127 genes with annotated protein sequences from the TIGR04052 family, downloaded from the JGI/IMG database on 19 May 2020 (Dataset S1) (52). Similar to the previous analysis (16), initial sequence similarity networks were generated using the enzyme function initiative–enzyme similarity tool (EFI-EST) and trimmed on the basis of length with a cutoff to remove sequences with fewer than 249 or greater than 379 residues (53, 54). An E-value cutoff of 1E-70 was used, and sequences with 100% identity were clustered into single nodes, decreasing overrepresented sequences and yielding a final network with 556 EFI-EST representative nodes. The EFI-EST representative nodes were then correlated with the input list of proteins and the amino acid sequences for only the representative nodes were retrieved (Dataset S2). A trimmed input file of EFI-EST–generated representative nodes at 50% identity was aligned using MAFFT (in L-INS-I mode) (55). This alignment was used to construct a new hidden Markov model (HMM) (Dataset S3) via hmmbuild, and hmmalign was used to align the sequences against the profile HMM (56, 57). This model was used to generate a sequence conservation logo. Conservation information was added to the sequence similarity network (SSN) metadata and visualized (Dataset S4).

To investigate the genomic neighborhood of MbnP, metadata were obtained for all genes annotated with specific PFAM and TIGRFAM families within five genes (upstream and downstream) of MbnP that occur in >2.5% of the MbnP neighborhoods (Dataset S5). Hierarchical clustering of MbnP genes against these traits was then carried out as described previously (Dataset S6) (55). Briefly, clustering was calculated in R using the Manhattan method (absolute distance) in the dist function to calculate the distance matrix (58). Clustering was determined using the Ward.D2 method in the hclust function (59). To generate dendrograms and a heat map from the hierarchical clustering data, the heatmap.2 function in gplots was used (60). Coclustered sets of traits were determined using a cluster cutoff to establish 10 primary operon groups. Ten randomly selected MbnP gene_oids from each of the 10 operon families were checked visually using the JGI/IMG genomic database to manually confirm the clustering results.

Expression and Purification of MbnP and $MbnP^H$. To heterologously overexpress MbnP, two constructs were designed. The first construct encodes only MbnP, and the second allows for coexpression of MbnP with MbnH, denoted $MbnP^H$. The codon-optimized *mbnH* gene (MettrDRAFT_3427) and its neighboring *mbnP* gene (MettrDRAFT_3426) from *Ms. trichosporium* OB3b were cloned into separate pCDFDuet-1 vectors as well as the same pCDFDuet-1 vector to generate the two constructs. The gene for codon-optimized *mbnP* was modified to contain either a C-terminal His_6-tag with a tobacco etch virus (TEV) cleavage site or a C-terminal Strep tag and inserted into MCS-1. The gene for *mbnH* was modified to contain a C-terminal Strep tag or a C-terminal His_6-tag with a TEV cleavage site and inserted into MCS-2. Since both proteins are predicted to be periplasmic, the native methanotrophic periplasmic signal sequence was replaced with the *Escherichia coli* PelB periplasmic targeting sequence to ensure proper export to the periplasm. Likewise, to improve incorporation of *c*-type hemes into MbnH during aerobic expression, the modified pCDFDuet-1 vector was cotransformed with a pEC86 vector (containing the cytochrome *c* maturation or *ccm* genes) into BL21-DE3* cells (61, 62). An MbnH mutant in which Glu136 is replaced by a glutamine residue was also constructed using site-directed mutagenesis. This third construct contained the E136Q MbnH gene in MCS-2 and the wild-type MbnP gene in MCS-1.

A single colony was picked from a freshly transformed plate and grown at 37 °C for 14 h in 5 mL of Luria Broth (LB) media. This initial culture was then used to inoculate a 100-mL LB starter culture that was grown at 37 °C, 180 rpm for 4 h. Next, 10 mL of starter culture was used to inoculate 1 L of ZYM-5052 autoinduction media as described previously (63). Cells were grown to an optical density at 600 nm of 0.4 at 37 °C prior to lowering the temperature for 12 to 14 h of expression at 18 °C. Cells were harvested via centrifugation at 6,800 × *g* for 10 min, and the wet pellets were combined and frozen at −80 °C until lysis. For lysis, cells were thawed completely to room temperature in 3 mL of lysis buffer (25 mM Tris, pH 7.4, and 100 mM NaCl) for every 1 g of cell pellet in the presence of DNase and 1 mM phenylmethylsulfonyl fluoride. Once thawed, cells were passed through the chilled disruptor of a microfluidizer three times, and the resulting lysate was clarified by centrifugation at 125,000 × *g* for 40 min in a Beckman Coulter Optima XE 90 analytical ultracentrifuge. The supernatant was poured off and filtered through a 0.45-μm syringe filter prior to protein purification.

His-tagged MbnP was purified using standard affinity chromatography on a Ni-loaded HiTrap Chelating column (GE Healthcare). The His-tagged MbnP or $MbnP^H$ was eluted with a 25 mM Tris, pH 7.4, and 100 mM NaCl buffer containing 1 M imidazole over a 10 to 50% gradient. A single peak was isolated, and the protein was exchanged into 25 mM Tris, pH 7.4, and 100 mM NaCl and concentrated to 1 mL for further purification on a Superdex 75 or Superdex 200 column (120 mL; GE Healthcare). For Strep-tagged MbnP, protein was loaded onto a self-packed, high-capacity Strep-tactin Superflow column (IBA Lifesciences) and eluted using 25 mM Tris, pH 7.4,100 mM NaCl, and 2.5 mM *d*-desthiobiotin. A single peak was isolated, and the protein was exchanged into 25 mM Tris, pH 7.4, and 100 mM NaCl and concentrated to 1 mL for further purification on a Superdex 75 column (120 mL; GE Healthcare). Protein purity was assessed by SDS polyacrylamide gel electrophoresis (*SI Appendix*, Fig. S1). If necessary, further purification was performed using a self-packed source 30Q anion exchange column to remove residual contaminants. The extinction coefficients of MbnP and $MbnP^H$ were determined using the Bradford assay (64). Tag-free proteins were prepared by cleaving the His tag from pure $MbnP^H$ using TEV protease. A 1:20 (TEV:$MbnP^H$) mixture was incubated for 14 h at 4 °C. Following cleavage, the protein was applied to a Ni column to remove the cleaved His-tag, and the tag-free protein that did not bind to the column was collected.

Metal-Binding Analysis of $MbnP^H$. ICP-MS analysis was conducted at the Quantitative Bio-element Imaging Center at Northwestern University. Quantification of calcium (Ca), iron (Fe), and copper (Cu) was performed using samples digested in concentrated trace nitric acid (> 69%; Thermo Fisher Scientific) and placed at 65 °C overnight for ∼14 h. Ultrapure H_2O (18.2 MΩ·cm) was then added to produce a final solution of 3.0% nitric acid (vol/vol) in a total sample volume of 10 mL. A 100 μg/mL mixed element standard containing Ca, Fe, and Cu (Inorganic Ventures) was used to create a 100 ng/mL mixed element quantitative standard in 3.0% nitric acid (vol/vol) in a total sample volume of 50 mL. Samples were measured using a Thermo iCapQ ICP-MS (Thermo Fisher Scientific) controlled by the QTEGRA software. The ICP-MS was operating in KED mode and equipped with an ESI SC-2DX prepFAST autosampler. Internal standard was added inline using the prepFAST system and consisted of 1 ng/mL of a mixed element solution containing Bi, In, ^{6}Li, Sc, Tb, Y (IV-ICPMS-71D from Inorganic Ventures). Online dilution was also carried out by the prepFAST system and used to generate calibration curves consisting of 100, 50, 10, 2, 1, and 0.5 ng/g Ca, Fe, and Cu. Each sample was measured using one survey run (10 sweeps) and three main runs (40 sweeps). The isotopes selected for analysis were ^{44}Ca, ^{56}Fe, ^{57}Fe, ^{63}Cu, ^{65}Cu, ^{89}Y, and ^{115}In (chosen as internal standards for data interpolation and machine stability).

The Cu^I dissociation constant (K_d) of $MbnP^H$ was estimated using the Cu^I chelator BCS. To ensure that any copper present was kept in the Cu^I oxidation state, 4 equivalents of ascorbate were added to the protein solution prior to BCS addition. BCS was added in 0.5- to 1-μL aliquots to a sample of ∼12 μM $MbnP^H$ in 25 mM Tris, pH 7.5, and 100 mM NaCl. After the addition of each titrant, the sample was equilibrated at room temperature for 20 min prior to collecting an absorbance spectrum. Transfer of Cu^I from $MbnP^H$ to BCS to form $[Cu^I(BCS)_2]^{3-}$ was established by monitoring the change in absorbance at 483 nm (ε = 12,500 $M^{-1}\cdot cm^{-1}$) (26, 28, 65) using a buffer reference. A sample containing only buffer, ascorbate, and BCS was used as a control at each titrant. Each spectrum was corrected by subtraction of the control sample and normalized for dilution. A K_d value for Cu^I binding in $MbnP^H$ was established using Eqs. 1–**3**, modeled after reaction 1:

$$Cu^{I} - MbnP + 2BCS \rightleftharpoons MbnP + \left[Cu^{I}(BCS)_2\right]^{3-} \text{ (reaction 1)}$$

$$K_{a,\,apparent} = \frac{[MbnP]\left[\left[Cu^{I}(BCS)_2\right]^{3-}\right]}{[Cu^{I} - MbnP][2BCS]^2} \quad [1]$$

$$K_{d,\,apparent} = \frac{[Cu^{I} - MbnP][2BCS]^2}{[MbnP]\left[\left[Cu^{I}(BCS)_2\right]^{3-}\right]} \quad [2]$$

$$K_{d,\,Cu^{I}-MbnP} = \frac{\beta_{\left[Cu(BCS)_2\right]^{3-}}}{K_{a,\,apparent}}. \quad [3]$$

In these equations, $K_{a,apparent}$ is the apparent association constant for $[Cu^{I}(BCS)_2]^{3-}$ as determined from experiment, $K_{d,apparent}$ is the apparent dissociation constant for $[Cu^{I}(BCS)_2]^{3-}$ as determined from experiment, [MbnP] and $[[Cu(BCS)_2]^{3-}]$ represent total concentrations in solution, and [BCS] represents the free concentration of ligand in solution. The overall association constant (β) for $[Cu^{I}(BCS)_2]^{3-}$ is pH-dependent, and a value of 6.1×10^{19} M^{-2} was used as reported previously for pH 7.5 (66). Calculations for the K_d of Cu^{I}-MbnP are shown in *SI Appendix*, Table S1.

SEC-MALS. The molar masses and solution oligomeric states of MbnP were determined using SEC-MALS in the Northwestern Keck Biophysics Facility. Purified MbnP or $MbnP^{H}$ samples containing a His_6-tag, Strep-tag, or cleaved His_6-tag were concentrated to 3 mg/mL using a 10-kDa molecular weight cutoff (MWCO) centricon (Millipore). Samples were analyzed using an Agilent 1260 series high-performance liquid chromatography system equipped with diode array detection absorbance in-line with a DAWN HELEOS II multiangle static light scattering detector, a QELS dynamic light-scattering detector, and a T-rEx differential refractive index detector (Wyatt Technology). A Superdex 75 Increase 10/300 GL column (GE Healthcare) was equilibrated with 25 mM Tris, pH 7.4, and 100 mM NaCl before application of 300 μL protein. Prior to injection, both the buffer and protein sample were maintained at 4 °C on ice and the column was kept at 4 °C. Each sample was run at 0.4 mL·min^{-1} for 60 min. Optical spectra were recorded at the apex of each peak, and data were processed and analyzed using IgorPro 8 (Wavemetrics).

Measurement of Fluorescence Spectra. MbnP, $MbnP^{H}$, $MbnP^{E136Q\ H}$, W174Y $MbnP^{H}$, and W176Y $MbnP^{H}$ samples were purified as described above. Protein samples were then exchanged into 25 mM MES, pH 6.4, with 100 mM NaCl and treated with 100-fold excess of DTT and BCS in the presence of 1% SDS, which allowed for unfolding of the protein sample and near-quantitative copper removal. Excess DTT, SDS, and $[Cu(BCS)_2]^{3-}$ were removed using a PD10 column (GE Healthcare), and fractions containing protein were concentrated using a 10-kDa MWCO centricon. Concentrated protein was then applied to a second PD10 column as a final clean-up step and concentrated once more. The resultant sample were submitted for ICP-MS analysis to validate that copper was removed. Denatured, copper-free fluorescence samples were then prepared by diluting the protein to an approximate concentration of 50 μM. All fluorescence spectra were collected at 4 °C on an ISS PC1 spectrofluorimeter using a 295-nm cutoff filter to avoid complications from tryptophan emission. Excitation was performed using the published excitation wavelength for kynurenine of 365 nm, an emission range of 400 to 600 nm, and a time base of 1 s. Excitation scans were collected by holding the emission at 450 nm and scanning an excitation wavelength range of 300 to 420 nm to validate the excitation maximum.

Crystallization and Structure Determination. Crystals of the copper-bound dimeric $MbnP^{H}$ species were obtained at 4 °C using 5 mg/mL protein in the $AmSO_4$ Suite (Qiagen) condition B6 (0.2 M lithium chloride and 2.2 M ammonium sulfate). Crystallization conditions were further optimized by varying the concentration of ammonium sulfate, and the crystal used for data collection was obtained from sitting-drop screens with 0.2 M lithium chloride and 1.6 M ammonium sulfate. Prior to data collection, the crystal was soaked for 2 to 5 min in a cryoprotectant solution consisting of the crystallization solution supplemented with 10% ethylene glycol and then submerged in liquid nitrogen. Data were collected at 77 K at a wavelength of 1.377 Å at the LS-CAT beamline 21 ID-D at the Advanced Photon Source at Argonne National Laboratory. The crystals belong to space group $P6_1$ with six $MbnP^{H}$ monomers in the asymmetric unit.

The data were processed using xia2 (67) to 2.04-Å resolution (*SI Appendix*, Table S2). The structure was solved using the SAD method with phenix.autosol (68), and phenix.autobuild was used to obtain an initial model that included six protein chains. This model was improved through iterative rounds of model building using Coot (69) and refinement using phenix.refine, resulting in a final R/R_{free} value of 20.4%/24.9% (*SI Appendix*, Table S2). The Molprobity score (70) is 1.53 and the clashscore is 5.02. The final model includes 1,743 residues (amino acids 29 to 321 in chain A, amino acids 28 to 316 in chain B, amino acids 29 to 316 in chain C, amino acids 28 to 315 in chain D, amino acids 29 to 323 in chain E, and amino acids 29 to 319 in chain F), 6 Cu ions, 6 Ca ions, 19 sulfate ions, 36 ethylene glycol molecules, and 582 water molecules. The Ramachandran plot indicates that 96.09% of residues are in favored regions with the remaining 3.91% in allowed regions.

EPR Spectroscopy. The as-isolated $MbnP^{H}$ sample was prepared by concentrating purified $MbnP^{H}$ to a final concentration of ~300 μM protein in 25 mM Tris pH 7.4, and 100 mM NaCl. The sample was then transferred into a Wilmad quartz X-band EPR tube (Sigma-Aldrich) and frozen in liquid nitrogen until analysis. For H_2O_2-treated $MbnP^{H}$ samples, a final concentration of 16 mM H_2O_2 was added to a ~300 μM protein sample in 25 mM Tris, pH 7.4, and 100 mM NaCl. For oxidation with K_2IrCl_6, a 50 mM solution of K_2IrCl_6 in 50 mM sodium acetate, pH 5.0, was prepared and used to make a 10 mM working solution in 25 mM Tris, pH 7.4, and 100 mM NaCl. To oxidize $MbnP^{H}$, a series of samples was prepared in which a final concentration of 0.8 mM $MbnP^{H}$ was mixed with 2.4 mM, 4 mM, or 8 mM K_2IrCl_6 in 25 mM Tris, pH 7.4, and 100 mM NaCl. The potential of each sample was measured using a voltmeter and a two-electrode system with an Ag/AgCl reference electrode and a GC working electrode. The samples were then transferred to custom quartz Q-band tubes and frozen in liquid nitrogen until analysis. All CW X-band spectra were acquired on a Bruker ESP-300 spectrometer with a liquid helium flow Oxford Instruments ESR-900 cryostat at 20 K using a modulation amplitude of 12.5 G. A CW Q-band spectra of 4mM K_2IrCl_6 oxidized $MbnP^{H}$ was acquired on a Bruker EMX spectrometer with an Oxford Instruments CF935 cryostat at 30 K with modulation of 4 G. A numerical derivative of the collected spectra was calculated for better presentation and analysis of the *g*-tensors and copper hyperfine splitting. Spin quantitation was carried out at Q-band using a Cu^{II}EDTA spin standard. Standards of 50 μM, 100 μM, 250 μM, 500 μM, and 1 mM Cu^{II} were prepared in 10-mL volumetric flasks containing 100 mM sodium chloride in milliQ water with 5% more ethylenediaminetetraacetic acid than copper to ensure full chelation. One hundred microliters of each standard solution was aliquoted into a Q-Band tube and flash-frozen in liquid nitrogen. For quantitation, the Cu^{II} $MbnP^{H}$ spectrum was first simulated using EasySpin (71). This simulation was then double-integrated and compared to a linear fit produced from the standards.

Data Availability. The atomic coordinates and structure factors have been deposited in the Protein Data Bank with accession number 7L6G. All other study data are included in the article and supporting information.

ACKNOWLEDGMENTS. This work was supported by NIH grants GM118035 (A.C.R.), GM111097 (B.M.H.), and T32GM008382 (R.J.J.), NSF grant MCB1515981 (B.M.H.), and a Simons Foundation Award through the Life Sciences Research Foundation (A.C.M.). Metal analysis was performed at the Northwestern University Quantitative Bio-element Imaging Center generously supported by NASA Ames Research Center Grant NNA04CC36G. SEC-MALS analysis was performed by the Northwestern Keck Biophysics Facility. This work utilized the LS-CAT beamlines of the Advanced Photon Source, which is a United States Department of Energy (DOE) Office of Science User Facility operated for the DOE Office of Science by Argonne National Laboratory under Contract DE-AC02-06CH11356. Use of LS-CAT Sector 21 was supported by the Michigan Economic Development Corporation and the Michigan Technology Tri-Corridor (Grant 085P1000817). We acknowledge staff and instrumentation support from the Structural Biology Facility at Northwestern University, the Robert H. Lurie Comprehensive Cancer Center of Northwestern University, and National Cancer Institute Cancer Center Support Grant P30 CA060553. We thank Zdzislaw Wawrzak for assistance with crystallographic data analysis. Cell lysis was accomplished using a microfluidizer in the Pinkett laboratory at Northwestern University, and A.C.M. thanks Dr. Grace Kenney and Professor Michael Stevenson for helpful insight and discussions.

1. J. D. Semrau, A. A. DiSpirito, S. Yoon, Methanotrophs and copper. *FEMS Microbiol. Rev.* **34**, 496–531 (2010).
2. S. Sirajuddin, A. C. Rosenzweig, Enzymatic oxidation of methane. *Biochemistry* **54**, 2283–2294 (2015).
3. R. Banerjee, J. C. Jones, J. D. Lipscomb, Soluble methane monooxygenase. *Annu. Rev. Biochem.* **88**, 409–431 (2019).
4. J. C. Murrell, I. R. McDonald, B. Gilbert, Regulation of expression of methane monooxygenases by copper ions. *Trends Microbiol.* **8**, 221–225 (2000).
5. D. W. Choi *et al*., The membrane-associated methane monooxygenase (pMMO) and pMMO-NADH:quinone oxidoreductase complex from *Methylococcus capsulatus* Bath. *J. Bacteriol.* **185**, 5755–5764 (2003).
6. S. Sirajuddin *et al*., Effects of zinc on particulate methane monooxygenase activity and structure. *J. Biol. Chem.* **289**, 21782–21794 (2014).
7. G. E. Kenney, A. C. Rosenzweig, Methanobactins: Maintaining copper homeostasis in methanotrophs and beyond. *J. Biol. Chem.* **293**, 4606–4615 (2018).
8. G. E. Kenney, M. Sadek, A. C. Rosenzweig, Copper-responsive gene expression in the methanotroph *Methylosinus trichosporium* OB3b. *Metallomics* **8**, 931–940 (2016).
9. W. Gu *et al*., A TonB-dependent transporter is responsible for methanobactin uptake by *Methylosinus trichosporium* OB3b. *Appl. Environ. Microbiol.* **82**, 1917–1923 (2016).
10. L. M. K. Dassama, G. E. Kenney, S. Y. Ro, E. L. Zielazinski, A. C. Rosenzweig, Methanobactin transport machinery. *Proc. Natl. Acad. Sci. U.S.A.* **113**, 13027–13032 (2016).
11. A. Baslé, A. El Ghazouani, J. Lee, C. Dennison, Insight into metal removal from peptides that sequester copper for methane oxidation. *Chemistry* **24**, 4515–4518 (2018).
12. L. M. K. Dassama, G. E. Kenney, A. C. Rosenzweig, Methanobactins: From genome to function. *Metallomics* **9**, 7–20 (2017).
13. Y. J. Park, G. E. Kenney, L. F. Schachner, N. L. Kelleher, A. C. Rosenzweig, Repurposed HisC aminotransferases complete the biosynthesis of some methanobactins. *Biochemistry* **57**, 3515–3523 (2018).
14. G. E. Kenney *et al*., The biosynthesis of methanobactin. *Science* **359**, 1411–1416 (2018).
15. B. D. Krentz *et al*., A comparison of methanobactins from *Methylosinus trichosporium* OB3b and *Methylocystis* strain Sb2 predicts methanobactins are synthesized from diverse peptide precursors modified to create a common core for binding and reducing copper ions. *Biochemistry* **49**, 10117–10130 (2010).
16. G. E. Kenney *et al*., MbnH is a diheme MauG-like protein associated with microbial copper homeostasis. *J. Biol. Chem.* **294**, 16141–16151 (2019).
17. J. Geng, I. Davis, F. Liu, A. Liu, Bis-Fe(IV): Nature's sniper for long-range oxidation. *J. Biol. Inorg. Chem.* **19**, 1057–1067 (2014).
18. J. Geng, K. Dornevil, V. L. Davidson, A. Liu, Tryptophan-mediated charge-resonance stabilization in the bis-Fe(IV) redox state of MauG. *Proc. Natl. Acad. Sci. U.S.A.* **110**, 9639–9644 (2013).
19. N. A. Tarboush *et al*., Mutagenesis of tryptophan199 suggests that hopping is required for MauG-dependent tryptophan tryptophylquinone biosynthesis. *Proc. Natl. Acad. Sci. U.S.A.* **108**, 16956–16961 (2011).
20. G. E. Kenney, A. C. Rosenzweig, Chalkophores. *Annu. Rev. Biochem.* **87**, 645–676 (2018).
21. K. A. Johnson *et al*., CorA is a copper repressible surface-associated copper(I)-binding protein produced in *Methylomicrobium album* BG8. *PLoS One* **9**, e87750 (2014).
22. R. Helland *et al*., An oxidized tryptophan facilitates copper binding in *Methylococcus capsulatus*-secreted protein MopE. *J. Biol. Chem.* **283**, 13897–13904 (2008).
23. T. Ve *et al*., The *Methylococcus capsulatus* (Bath) secreted protein, MopE*, binds both reduced and oxidized copper. *PLoS One* **7**, e43146 (2012).
24. V. N. Shchukin, V. N. Khmelenina, B. Ts. Eshinimaev, N. E. Suzina, IuA. Trotsenko, [Primary characterization of dominant cell surface proteins of halotolerant methanotroph *Methylomicrobium alcaliphilum* 20Z]. *Mikrobiologiia* **80**, 595–605 (2011).
25. O. Berson, M. E. Lidstrom, Cloning and characterization of corA, a gene encoding a copper-repressible polypeptide in the type I methanotroph, *Methylomicrobium albus* BG8. *FEMS Microbiol. Lett.* **148**, 169–174 (1997).
26. Z. Xiao, F. Loughlin, G. N. George, G. J. Howlett, A. G. Wedd, C-terminal domain of the membrane copper transporter Ctr1 from *Saccharomyces cerevisiae* binds four Cu(I) ions as a cuprous-thiolate polynuclear cluster: Sub-femtomolar Cu(I) affinity of three proteins involved in copper trafficking. *J. Am. Chem. Soc.* **126**, 3081–3090 (2004).
27. D. K. Johnson *et al*., Stabilization of Cu(I) for binding and calorimetric measurements in aqueous solution. *Dalton Trans.* **44**, 16494–16505 (2015).
28. Z. Xiao *et al*., Unification of the copper(I) binding affinities of the metallo-chaperones Atx1, Atox1, and related proteins: Detection probes and affinity standards. *J. Biol. Chem.* **286**, 11047–11055 (2011).
29. Y. Fukunaga, Y. Katsuragi, T. Izumi, F. Sakiyama, Fluorescence characteristics of kynurenine and N′-formylkynurenine their use as reporters of the environment of tryptophan 62 in hen egg-white lysozyme. *J. Biochem.* **92**, 129–141 (1982).
30. W. G. Lesniak *et al*., Concurrent quantification of tryptophan and its major metabolites. *Anal. Biochem.* **443**, 222–231 (2013).
31. L. V. Sinclair, D. Neyens, G. Ramsay, P. M. Taylor, D. A. Cantrell, Single cell analysis of kynurenine and System L amino acid transport in T cells. *Nat. Commun.* **9**, 1981 (2018).
32. E. Krissinel, K. Henrick, Inference of macromolecular assemblies from crystalline state. *J. Mol. Biol.* **372**, 774–797 (2007).
33. W. Yang, H.-W. Lee, H. Hellinga, J. J. Yang, Structural analysis, identification, and design of calcium-binding sites in proteins. *Proteins* **47**, 344–356 (2002).
34. J. Peisach, W. E. Blumberg, Structural implications derived from the analysis of electron paramagnetic resonance spectra of natural and artificial copper proteins. *Arch. Biochem. Biophys.* **165**, 691–708 (1974).
35. K. Katoh, D. M. Standley, MAFFT multiple sequence alignment software version 7: Improvements in performance and usability. *Mol. Biol. Evol.* **30**, 772–780 (2013).
36. W. R. Pearson, An introduction to sequence similarity ("homology") searching. *Curr. Protoc. Bioinformatics* **Chap. 3**, Unit 3.1 (2013).
37. R. Balamurugan, M. Palaniandavar, R. S. Gopalan, Trigonal planar copper(I) complex: Synthesis, structure, and spectra of a redox pair of novel copper(II/I) complexes of tridentate bis(benzimidazol-2′-yl) ligand framework as models for electron-transfer copper proteins. *Inorg. Chem.* **40**, 2246–2255 (2001).
38. J. P. Naskar, S. Chowdhury, M. G. B. Drew, D. Datta, Chemistry of the copper(I)–water bond. Some new observations. *New J. Chem.* **26**, 170–175 (2002).
39. L. A. López, P. Barrio, J. Borge, Cationic copper(I) carbene complexes: Synthesis and structures of a tricoordinate copper(I) carbene water complex and a dicoordinate carbene complex. *Organometallics* **31**, 7844–7848 (2012).
40. C. Dash, A. Das, M. Yousufuddin, H. V. R. Dias, Isolable, copper(I) dicarbonyl complexes supported by *N*-heterocyclic carbenes. *Inorg. Chem.* **52**, 1584–1590 (2013).
41. J. T. Rubino, K. J. Franz, Coordination chemistry of copper proteins: How nature handles a toxic cargo for essential function. *J. Inorg. Biochem.* **107**, 129–143 (2012).
42. Y. Fu, F.-M. J. Chang, D. P. Giedroc, Copper transport and trafficking at the host-bacterial pathogen interface. *Acc. Chem. Res.* **47**, 3605–3613 (2014).
43. A. V. Davis, T. V. O'Halloran, A place for thioether chemistry in cellular copper ion recognition and trafficking. *Nat. Chem. Biol.* **4**, 148–151 (2008).
44. M. M. Harding, Geometry of metal-ligand interactions in proteins. *Acta Crystallogr. D Biol. Crystallogr.* **57**, 401–411 (2001).
45. M. M. Harding, Small revisions to predicted distances around metal sites in proteins. *Acta Crystallogr. D Biol. Crystallogr.* **62**, 678–682 (2006).
46. Z.-M. Wang *et al*., catena-Poly. *Acta Crystallogr. C* **56**, 786–788 (2000).
47. A. El Ghazouani *et al*., Copper-binding properties and structures of methanobactins from *Methylosinus trichosporium* OB3b. *Inorg. Chem.* **50**, 1378–1391 (2011).
48. N. Bandow *et al*., Spectral and copper binding properties of methanobactin from the facultative methanotroph *Methylocystis* strain SB2. *J. Inorg. Biochem.* **110**, 72–82 (2012).
49. M.-L. Pesch, I. Christl, M. Hoffmann, S. M. Kraemer, R. Kretzschmar, Copper complexation of methanobactin isolated from *Methylosinus trichosporium* OB3b: pH-dependent speciation and modeling. *J. Inorg. Biochem.* **116**, 55–62 (2012).
50. G. E. Kenney, A. C. Rosenzweig, Genome mining for methanobactins. *BMC Biol.* **11**, 17 (2013).
51. L. A. Abriata *et al*., Mechanism of Cu_A assembly. *Nat. Chem. Biol.* **4**, 599–601 (2008).
52. I. A. Chen *et al*., IMG/M v.5.0: An integrated data management and comparative analysis system for microbial genomes and microbiomes. *Nucleic Acids Res.* **47** (D1), D666–D677 (2019).
53. J. A. Gerlt, Genomic enzymology: Web tools for leveraging protein family sequence–function space and genome context to discover novel functions. *Biochemistry* **56**, 4293–4308 (2017).
54. J. A. Gerlt *et al*., Enzyme function initiative-enzyme similarity tool (EFI-EST): A web tool for generating protein sequence similarity networks. *Biochim. Biophys. Acta* **1854**, 1019–1037 (2015).
55. T. J. Lawton, G. E. Kenney, J. D. Hurley, A. C. Rosenzweig, The CopC family: Structural and bioinformatic insights into a diverse group of periplasmic copper binding proteins. *Biochemistry* **55**, 2278–2290 (2016).
56. R. D. Finn, J. Clements, S. R. Eddy, HMMER web server: Interactive sequence similarity searching. *Nucleic Acids Res.* **39**, W29-37 (2011).
57. S. C. Potter *et al*., HMMER web server: 2018 update. *Nucleic Acids Res.* **46**, W200–W204 (2018).
58. R. Ihaka, R. Gentleman, R: A language for data analysis and graphics. *J. Comput. Graph. Stat.* **5**, 299–314 (1996).
59. J. H. Ward, Hierarchical grouping to optimize an objective function. *J. Am. Stat. Assoc.* **58**, 236–244 (1963).
60. G. R. Warnes *et al*., gplots: Various R programming tools for plotting data (2020).
61. E. Arslan, H. Schulz, R. Zufferey, P. Künzler, L. Thöny-Meyer, Overproduction of the *Bradyrhizobium japonicum* c-type cytochrome subunits of the cbb_3 oxidase in *Escherichia coli*. *Biochem. Biophys. Res. Commun.* **251**, 744–747 (1998).
62. C. Sanders, S. Turkarslan, D.-W. Lee, F. Daldal, Cytochrome *c* biogenesis: The Ccm system. *Trends Microbiol.* **18**, 266–274 (2010).
63. F. W. Studier, "Stable expression clones and auto-induction for protein production in *E. coli*" in *Structural Genomics: General Applications*, Y. W. Chen, Ed. (Methods in Molecular Biology, Humana Press, 2014), pp. 17–32.
64. M. M. Bradford, A rapid and sensitive method for the quantitation of microgram quantities of protein utilizing the principle of protein-dye binding. *Anal. Biochem.* **72**, 248–254 (1976).
65. A. Badarau, C. Dennison, Copper trafficking mechanism of CXXC-containing domains: Insight from the pH-dependence of their Cu(I) affinities. *J. Am. Chem. Soc.* **133**, 2983–2988 (2011).
66. A. Badarau, C. Dennison, Thermodynamics of copper and zinc distribution in the cyanobacterium *Synechocystis* PCC 6803. *Proc. Natl. Acad. Sci. U.S.A.* **108**, 13007–13012 (2011).
67. G. Winter, *xia2* : An expert system for macromolecular crystallography data reduction. *J. Appl. Cryst.* **43**, 186–190 (2010).
68. T. C. Terwilliger *et al*., Decision-making in structure solution using Bayesian estimates of map quality: The *PHENIX AutoSol* wizard. *Acta Crystallogr. D Biol. Crystallogr.* **65**, 582–601 (2009).
69. P. Emsley, K. Cowtan, Coot: Model-building tools for molecular graphics. *Acta Crystallogr. D Biol. Crystallogr.* **60**, 2126–2132 (2004).
70. C. J. Williams *et al*., MolProbity: More and better reference data for improved all-atom structure validation. *Protein Sci.* **27**, 293–315 (2018).
71. S. Stoll, A. Schweiger, EasySpin, a comprehensive software package for spectral simulation and analysis in EPR. *J. Magn. Reson.* **178**, 42–55 (2006).